catalysts

MDPI

Article

Preparation of Pt–Ru/C as an Oxygen-Reduction Electrocatalyst in Microbial Fuel Cells for Wastewater Treatment

Gaixiu Yang [1,2,3], Yongming Sun [1,2,*], Pengmei Lv [1,2], Feng Zhen [1,2], Xinyue Cao [1,2], Xiaojie Chen [1,2], Zhongming Wang [1,2], Zhenhong Yuan [1,2] and Xiaoying Kong [1,2,*]

1 Key Laboratory of Renewable Energy, Guangzhou Institute of Energy Conversion, Chinese Academy of Sciences, No. 2 Nengyuan Road, Tianhe, Guangzhou 510640, China; yanggx@ms.giec.ac.cn (G.Y.); Lvpm305@163.com (P.L.); zhenfeng304@163.com (F.Z.); caoxy@ms.giec.ac.cn (X.C.); chen1970@163.com (X.C.); xicaiming@126.com (Z.W.); yuanzh@ms.giec.ac.cn (Z.Y.)

2 Guangdong Key Laboratory of New and Renewable Energy Research and Development, Guangzhou Institute of Energy Conversion, Chinese Academy of Sciences, No. 2 Nengyuan Road, Tianhe, Guangzhou 510640, China

3 School of Environmental Science and Technology State Key Laboratory of Engines, Tianjin University, Tianjin 300072, China

* Correspondence: sunym@ms.giec.ac.cn (Y.S.); kongxy@ms.giec.ac.cn (X.K.); Tel.: +86-20-3702-9696 (Y.S. & X.K.); Fax: +86-20-3702-9689 (Y.S. & X.K.)

Academic Editor: Hong Liu
Received: 16 August 2016; Accepted: 20 September 2016; Published: 26 September 2016

Abstract: Carbon-supported Pt–Ru alloys with a Pt/Ru ratio of 1:1 were prepared by $NaBH_4$ reduction at room temperature. X-ray diffraction (XRD) measurements indicate that the as-prepared Pt–Ru nanoparticles had a face-centered cubic (fcc) structure. X-ray photoelectron spectroscopy (XPS) analyses demonstrate that alloying with Ru can decrease the 4f electron density of Pt, which results in a positive binding energy shift of 0.2 eV for the Pt 4f peaks. The catalytic properties of the synthesized Pt–Ru alloy catalysts were compared with those of commercial Pt/C catalysts by linear sweep voltammetry (LSV). The results show that the mass activity of the oxygen reduction reaction (ORR) is enhanced by 2.3 times as much mass activity of Pt relative to the commercial Pt/C catalyst. Single-chambered microbial fuel cell tests also confirm that the Pt–Ru alloys as cathode catalysts have better performance than that of commercial Pt/C catalysts.

Keywords: Pt–Ru nanoparticles; oxygen reduction reaction; electrocatalyst; microbial fuel cell

1. Introduction

Microbial fuel cells (MFCs) are devices that convert the chemical energy stored in organic matters into electrical energy, using microorganisms as biocatalysts. In addition to producing energy, biological wastewater is also treated simultaneously during the conversion process in the MFCs. During the conversion process, an electron acceptor is employed to receive the electrons transferred from the anode and complete the electrical circuit. Oxygen is undoubtedly a superior electron acceptor compared to others such as potassium ferricyanide $K_3Fe(CN)_6$ and potassium permanganate ($KMnO_4$), owing to its lower cost, higher electron capture capability, and environmental compatibility. Thus, the oxygen reduction reaction (ORR) is one of the key processes in the conversion of chemical energy to electrical energy in MFCs [1]. Owing to the sluggish kinetics of the ORR, Pt is typically used as a catalyst to accelerate the oxygen reduction process and directly transform chemical energy into electricity. It seems that cathode catalysts for the ORR present a major challenge for the practical applications of MFCs [2]. However, the scarce supply of Pt and consequent high cost continue to be the main obstacles

for the large-scale commercialization of MFCs. Therefore, researchers have devoted considerable efforts towards developing catalysts for the ORR, which are highly stable, active, and cost-effective.

Recent studies have examined the application of bimetallic Pt alloys as oxygen reduction catalysts. The catalytic activity of Pt towards the ORR at the cathode can be improved by alloying it with transition metals such as Pd, Ru, and Ni [3]. Pt-based bi- or tri-metallic electrocatalysts such as Pt–Co [4], Pt–Ni [5] Pt–Cu [6], Pt–V [7], and Pt–Pd–Co [8] have been found to exhibit markedly higher electrocatalytic activities towards the ORR compared to Pt alone in low-temperature fuel cells. This enhanced catalytic effect has been explained by various models, such as the "electronic effect" [9], which suggest that the alloying element promotes the catalytic effect of Pt. Among the various Pt alloy catalysts used for the ORR, Pt–Ru alloys have been extensively studied. These catalysts show higher current density and more positive ORR onset potentials than Pt/C in the acidic as well as alkaline media [3,10,11]. Further, it has been observed that the electrocatalytic activity of the Pt–Ru/C catalyst towards the ORR is strongly dependent on factors such as the nature of components in the system, particle size, and morphology. Based on our previous investigations, we understand that increasing the alloying degree of the Pt–Ru/C catalyst is favorable for enhancing its electrocatalytic activity and stability. Up to now, the role of Ru in enhancing the catalytic activity of Pt in the Pt–Ru catalyst is not clear, and the catalytic activity of the Pt–Ru alloy towards the ORR at neutral pH has not been well studied.

In the present study, we fabricated a carbon-supported 20 wt % Pt–Ru catalyst with a high alloying degree and Pt/Ru atomic ratio of 1:1 by a simple chemical reduction method and compared its characteristics with commercially available 20 wt % Pt/C catalysts. The catalyst prepared in this study was characterized by X-ray diffraction (XRD), transmission electron microscopy (TEM), X-ray photoelectron spectroscopy (XPS), and energy dispersive X-ray spectroscopy (EDS), with the goal of understanding the effect of Pt–Ru composition on the ORR activity in the MFCs. The electrochemical activity and stability towards the ORR in both three electrode cells, as well as air–cathode single-chamber MFCs, were tested. The results show that the Pt–Ru/C nanoparticles with high catalytic activity towards the ORR is a promising catalyst in MFCs.

2. Results and Discussion

2.1. Physical Characterization

Figure 1 shows the typical XRD patterns of the Pt/C and Pt–Ru/C nanoparticles. Firstly, the diffraction peaks around 2θ values of 40°, 47°, 68°, and 82° could be attributed to the Pt (111), (200), (220), and (311) crystalline planes, respectively, and correspond to crystalline Pt with a face-centered cubic (fcc) structure (JCPDS Card No. 04-0802). This pattern indicates that metallic Pt nanocrystals were generated. Secondly, there is a slight positive shift in the positions of the diffraction peaks for the Pt–Ru/C catalyst compared with the corresponding peak positions for Pt/C. This indicates that Ru has penetrated into the Pt lattice, forming a Pt–Ru alloy in the former case [12].

The particle size and composition of Pt–Ru/C were analyzed by TEM and EDX, respectively. The composition of the catalyst determined by EDX analysis indicates the presence of both Pt and Ru (data not shown), and these results manifest that Pt and Ru were successfully reduced. Figure 2 presents TEM images of the Pt/C and Pt–Ru/C catalysts. The average size of the Pt–Ru/C (3.9 nm) nanoparticles was smaller than that of the Pt/C nanoparticles (8.2 nm), indicating that alloying with Ru favors an increase in the catalytic activity, because of the reduction in particle size. It has been reported that both the activity and reaction mechanism may be affected by particle size [13]. The smaller the particle size, the higher the catalytic activity would be. In addition, the TEM images suggest that both Pt and Pt–Ru nanoparticles are uniformly dispersed.

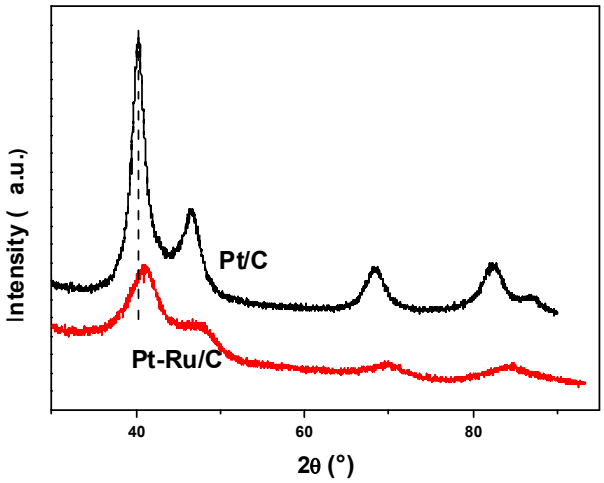

Figure 1. X-ray diffraction (XRD) patterns of the Pt/C and Pt–Ru/C catalysts.

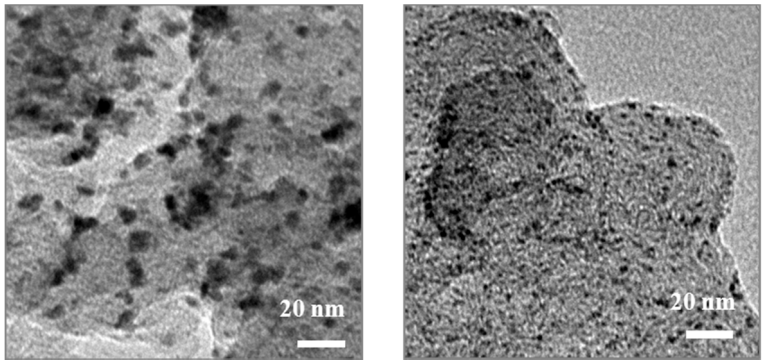

Figure 2. TEM images of (**a**) Pt/C; and (**b**) Pt–Ru/C catalysts.

Figure 3 shows the XPS spectra of the Pt–Ru/C and Pt/C catalysts in the Pt 4f and Ru 3p regions. Generally, the addition of Ru may lead to changes in the electronic structure of the Pt atoms owing to lattice strain [14]. As shown in Figure 3a, the 4f spectra of Pt in Pt–Ru alloys and commercial Pt/C catalyst can be deconvoluted into two pairs of doublets, in which the more intense doublet (at 71.9 and 75.2 eV for Pt in Pt–Ru/C and at 71.6 and 74.9 eV for Pt in Pt/C catalyst, respectively) corresponds to Pt^0. The second and weaker doublet, with binding energies (BEs) higher than those of Pt^0, could be assigned to Pt^{II} as in PtO and $Pt(OH)_2$ [15,16]. For Ru in Pt–Ru/C, one doublet at 463.2 and 486.0 eV corresponds to the zerovalent state of Ru.

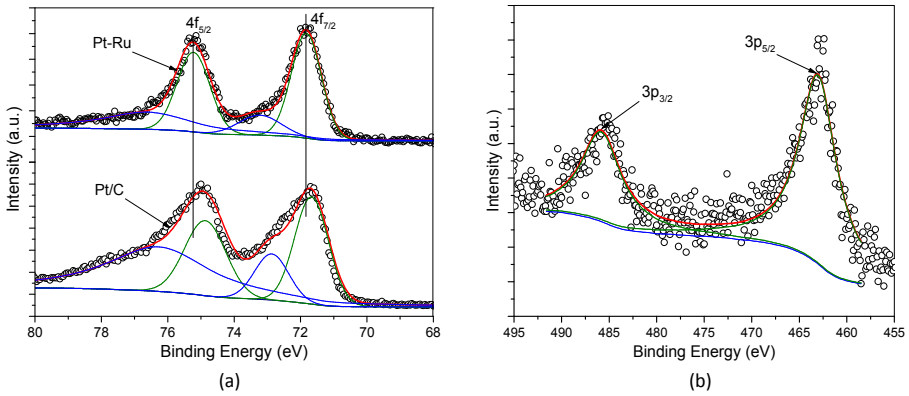

Figure 3. The 4f XPS spectra of Pt (**a**) in Pt–Ru/C and Pt/C catalysts and 3p XPS spectrum of Ru; (**b**) in the Pt–Ru/C catalyst.

Specifically, in comparison with the 4f peak positions of the commercial Pt/C catalyst, the 4f BEs of Pt in Pt–Ru/C clearly shifts to higher values, as indicated by Figure 3a, illustrating that the electronic structure of Pt has been modified by alloying with Ru. Besides particle size, the electronic interactions between the Pt and Ru atoms in Pt–Ru/C, as well as atomic composition, play an important role in determining the BE position for Pt $4f_{7/2}$ [17,18], as reported by Hu et al. [19]. The positive shift in Pt 4f BE means the decrease of electron density around the Pt atoms, which would be helpful in improving the adsorption of oxygen on the Pt sites, and hence promote the ORR [17,18,20].

2.2. Electrochemical Activity

We utilized a rotating disk electrode (RDE) to study the ORR activity of the catalysts. Figure 4 shows linear sweep voltammetries (LSVs) of the Pt–Ru/C and Pt/C nanoparticles in an oxygen-saturated 50-mM phosphate buffer solution (PBS). The onset potential for the current peak in the Pt–Ru/C catalyst was 0.48 V (vs. the reversible hydrogen electrode (RHE)), whereas the corresponding value for the commercial Pt/C catalyst was 0.45 V. (vs. the RHE). Thus, there is a slight positive peak shift for Pt–Ru/C compared to Pt/C. Based on this result, we hypothesize that the Pt sites act as the adsorption and reduction centers for oxygen.

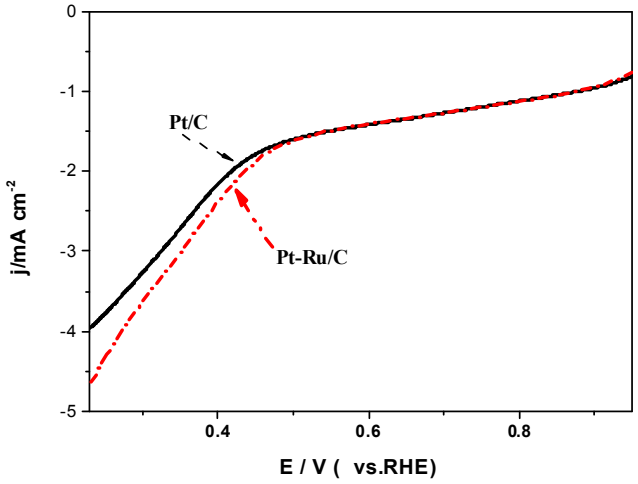

Figure 4. Linear sweep voltammetries (LSVs) of the Pt/C and Pt–Ru/C catalysts in the O_2-saturated pH-neutral electrolyte.

The π-bond of the adsorbed oxygen was weakened by the Ru atoms owing to the electronic coupling effect, which was supported by the XPS results. Further, alloying with Ru favors O–O bond breaking and O/OH hydrogenation [21,22]. Moreover, the addition of Ru is in favor of decreasing OH coverage on Pt, caused by lateral repulsion between the OH adsorbed on Pt and the OH or O adsorbed on a neighboring surface Ru atom. Hence, the ORR catalytic activity on Pt nanoparticles has been improved due to the strong adsorption of OH on Ru at low potentials [23].

To further demonstrate the efficiency of different catalysts towards the ORR in a neutral solution, the room-temperature performances of the MFCs containing Pt/C and Pt–Ru/C as cathode catalysts were assessed. Figure 5 shows the power densities and polarization curves of the MFCs with different cathodes. The results demonstrate that the maximum power density of the MFCs (Figure 5a) with a lower loading of Pt (Pt–Ru/C) as the cathode catalyst was 1139 $mW \cdot m^{-2}$, which was slightly higher than the corresponding value for Pt/C (985 $mW \cdot m^{-2}$). The maximum power densities generated in the MFCs are in a middle level compared with results in previous studies [4,24–27]. This enhancement in power density may be attributed to the synergistic effect of the addition of Ru (which improves the catalytic activity towards the ORR). A similar result was reported by Zardari et al. under alkaline conditions [3]. The polarization curves (Figure 5b) were obtained by determining the change in voltage as a function of current density. The electrode potential decreased with the increase in the current density. The non-linear polarization curves observed for the MFCs indicate that the decrease in the voltage was caused mainly by ohmic activation followed by the diffusion losses [28]. As observed from Figure 5b, the open-circuit potential of Pt–Ru/C (0.60 V) was 0.05 V higher than that of the Pt/C (0.55 V) catalyst. In contrast, the overpotential of the Pt–Ru/C catalyst was lower than that of the Pt catalyst. In addition, the Coulombic efficiency of the MFCs with Pt–Ru/C as cathode catalyst, calculated according to Equation (3), was 36.23% higher than that of the Pt/C catalyst, which exhibited a value of 32.39%.

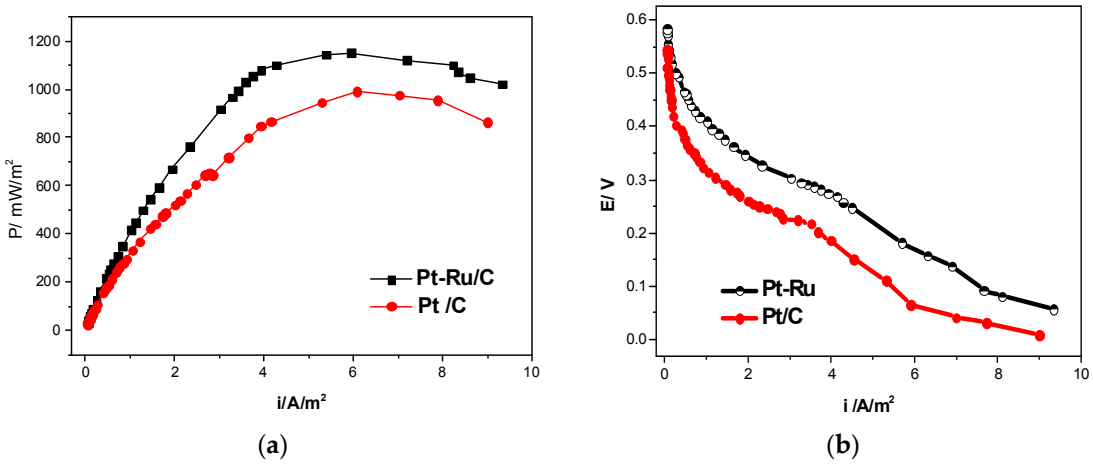

Figure 5. (**a**) Power density and (**b**) electrode polarization of the Pt–Ru/C and Pt/C cathode catalysts in the single-chamber microbial fuel cells (MFCs).

3. Experimental

3.1. The Preparation of Catalysts

The Pt–Ru electrocatalyst was prepared according to a method published in the literature [11]. Vulcan XC-72 (Shanghai Cabot Chemical Co. Ltd., Shanghai, China, BET surface area of 235 $m^2 \cdot g^{-1}$, denoted as C) was used as the carbon support. $H_2PtCl_6 \cdot 6H_2O$ and $RuCl_3$ were obtained from Shanghai July Chemical Co. (Shanghai, China) and were used as the Pt and Ru precursors, respectively. To prepare the Vulcan carbon-supported Pt–Ru catalyst, Vulcan carbon XC-72 (60 mg) was mixed with 1.1 mL of $H_2PtCl_6 \cdot 6H_2O$ (0.0193 M), 2.63 mL of $RuCl_3$ (0.048 M), and 12 mL of a solution containing

THF (6 mL), CH_3CH_2OH (4.8 mL), and H_2O (1.2 mL). The suspension obtained was sonicated for 1 h and then stirred for 20 h. Then, appropriate amounts of $NaBH_4$ and sodium carbonate were added, and the mixture was stirred for 1 h at 10 °C. Finally, after the suspension was filtered, washed, and dried in a vacuum oven at 60 °C for 10 h, the Pt–Ru/C catalyst containing 20 wt % Pt–Ru was obtained. The performance of this catalyst was compared to that of a commercial Pt/C catalyst (Shanghai July Chemical Co.) containing 20 wt % Pt/C.

3.2. Physical Characterization

The compositions of the catalysts were measured using an energy dispersive spectrometer from a Vantage Digital Acquisition Engine (Thermo Noran, Madison, WI, USA). The XPS measurements were carried out on a Kratos XSAM-800 spectrometer (Kratos, Manchester, UK) with Mg K_α radiation. The binding energy (BE) was calibrated with reference to the C 1s peak at 284.6 eV. The structural features of the prepared catalysts were studied via XRD (D-MAX 2200VPC, Rigaku, Tokyo, Japan) using Cu K_α radiation (λ = 0.15406 nm). TEM measurements were performed on a JEOL-2010 transmission electron microscope (JEOL, Tokyo, Japan)at an acceleration voltage of 200 kV.

3.3. Electrochemical Activity

The working electrode preparation and electrochemical measurement procedures were similar to those published in the literature [29]. The electrochemical measurements were performed using a conventional three-electrode electrochemical cell connected to a CHI 600 electrochemical analyzer (Shanghai Chenghua Co., Shanghai, China). A saturated calomel electrode (SCE) was used as the reference electrode, whereas Pt wire was the counter electrode. The Pt or Pt–Ru loading on the surface of the electrode was 28 $\mu g \cdot cm^{-2}$. All the chemicals used were of analytical grade. The electrochemical experiments were conducted with a 50-mM PBS as the electrolyte. LSVs were measured at a scan rate of 50 $mV \cdot s^{-1}$ between -0.2 and 0.8 V vs. SCE in an O_2 saturated PBS solution. The potentials were calibrated and converted to an RHE [30]. The electrolytes were deaerated by bubbling with high-purity nitrogen or oxygen. Additionally, a gentle nitrogen or oxygen flow was maintained above the surface of the electrolyte solutions during the measurements. All the electrochemical experiments were performed at 25 $\pm$ 5 °C.

3.4. Microbial Fuel Cell Measurements

3.4.1. MFC Construction and Electrode Preparation

An air–cathode single-chamber MFC with an inner volume of 40 cm^3 was constructed and is shown in Figure 6. PAN-carbon and graphite felt (5 cm $\times$ 2 cm $\times$ 0.5 cm) were used as the anode materials, whereas 20% Pt or 20% Pt–Ru was used as the cathode catalyst for the ORR with a loading of 0.5 $mg \cdot cm^{-2}$. Carbon cloth was used as the cathode material. The cathode was located on one side of the MFC with the ion-exchange film in direct contact with the anode electrolyte and the catalyst-coated layer facing air. All the anodes were first cleaned by dipping in pure acetone (Aladdin, Shanghai, China) overnight and were subsequently treated by soaking the carbon cloths in a solution consisting of concentrated sulfuric acid (100 $mL \cdot L^{-1}$) and ammonium peroxydisulfate (200 $g \cdot L^{-1}$) for 15 min. Ti wires were used as cathode and anode leads. The acrylic plates, electrodes, and the membrane were assembled along with a silicon gasket to prevent leakage. A 1000-Ω resistor was routinely used as the load resistor. Each experiment was performed twice.

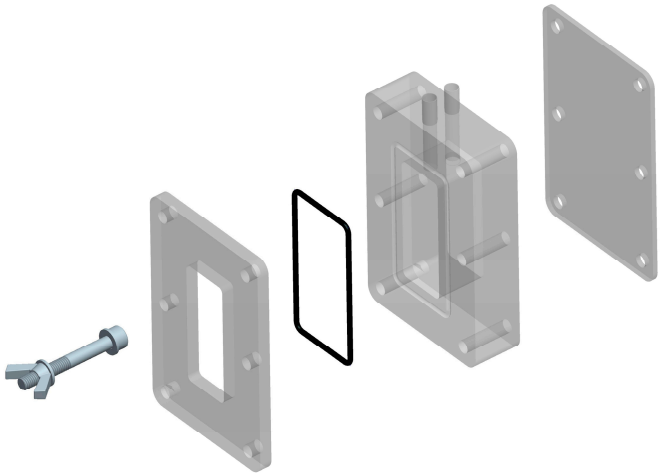

Figure 6. Illustration of the air cathode MFC Reactor.

3.4.2. Enrichment and Operation

All the MFCs were operated in the fed-batch mode. The cells were inoculated from a running MFC as a result of an enrichment transfer procedure over a period of three months in our laboratory, initiated from activated sludge that was obtained from the ZhuJiang River, Haizhu District, Guangzhou (Guangdong, China). Glucose (1 g·L^{-1}, 62.5 mL) and the culture media solution containing KH_2PO_4 (13.6 g·L^{-1}), NaOH (2.32 g·L^{-1}), NH_4Cl (0.31 g·L^{-1}), and NaCl (1.0 g·L^{-1}) were used to compose the artificial wastewater and added to the reactors [31,32]. The reactors were refilled by the artificial wastewater until the output voltage decreased to less than 50 mV. Thus, a complete operation cycle was formed.

3.4.3. Analytical Method

The power density was measured by varying the external resistance in the MFC circuit from 50 to 90,000 Ω. The external circuit voltage (E) was collected using a data-acquisition system connected to a computer (model ZP1001) from Guangzhou NXP Ltd. The current density (I) and power density (P) were calculated using Equations (1) and (2), respectively.

$$I = \frac{E}{RA}, \quad (1)$$

and

$$P = \frac{E^2}{RV}, \quad (2)$$

where R is the external resistance, A is the apparent area of the cathode material, and V is the volume of the anode chamber.

The Coulombic efficiency (CE) was calculated according to Equation (3).

$$CE = \frac{M\int_0^{t_b} idt}{FbV_{\mathrm{An}} \triangle \mathrm{COD}}, \quad (3)$$

where i is the current produced, V is the liquid volume (0.04 L), F is Faraday's constant (96485 C (mol of electrons)$^{-1}$), b is the number of moles of electrons produced per mole of O_2 (4 mol·mol^{-1}), M is the molar mass of O_2 (32 g·mol^{-1}), and [33] ΔCOD is the chemical oxygen demand (COD) on the difference in time t_b. The COD for glucose at a concentration of 1g·L^{-1} was assumed to be 1.063 g·L^{-1}.

All the aqueous samples from the MFCs were filtered through a membrane with a pore diameter of 0.22 mm to avoid interference from impurities. The filtrate was used for the determination of COD according to a standard method [34].

4. Conclusions

In this study, we successfully fabricated nanostructured Pt–Ru alloy catalysts with a Pt/Ru ratio of 1:1, by a $NaBH_4$ reduction at room temperature. The alloy catalysts were characterized by XRD, TEM, XPS, and EDS analyses. The results of these measurements revealed that the Pt–Ru alloy nanoparticles are ~3.9 nm in size, and the metal nanoparticles are dispersed uniformly on the carbon support. The electrochemical measurement results indicated that the Pt–Ru alloys possess 2.3 times as much mass activity of Pt towards the ORR compared with the commercial Pt/C catalyst. The Pt–Ru/C catalyst exhibited a higher activity owing to the synergistic effects from the decrease in Pt loading and doping with Ru. The above results clearly illustrate the role of Ru in the bimetallic catalyst and demonstrate that Pt–Ru/C is a promising substitute for Pt nanoparticles for the ORR in single chamber MFCs.

Acknowledgments: The research was supported by the Science and Technology Service Network Initiative (No. KFJ-Ew-STS-138) and Science and Technology Planning Project of Guangdong Province (No. 2015B020241002).

Author Contributions: Gaixiu Yang, Pengmei Lv, Feng Zhen, Xinyue Cao and Xiaojie Chen performed the materials synthesis, characterization, electrochemical measurement, and the MFC measurements. Gaixiu Yang wrote the main manuscript text, Zhenhong Yuan and Zhongming Wang, participated in the manuscript formatting. Xiaoying Kong and Yongming Sun supervised the project and revised the manuscript text, and all authors participated in the review of the manuscript.

Conflicts of Interest: The authors declare no conflict of interest.

References

1. Kannan, M.V.; Gnana Kumar, G. Current status, key challenges and its solutions in the design and development of graphene based orr catalysts for the microbial fuel cell applications. *Biosens. Bioelectron.* **2016**, *77*, 1208–1220. [CrossRef] [PubMed]
2. Yuan, H.; Hou, Y.; Abu-Reesh, I.M.; Chen, J.; He, Z. Oxygen reduction reaction catalysts used in microbial fuel cells for energy-efficient wastewater treatment: A review. *Mater. Horiz.* **2016**, *3*, 382–401. [CrossRef]
3. Hosseini, M.G.; Zardari, P. Electrocatalytical study of carbon supported Pt, Ru and bimetallic Pt–Ru nanoparticles for oxygen reduction reaction in alkaline media. *Appl. Surf. Sci.* **2015**, *345*, 223–231. [CrossRef]
4. Yan, Z.; Wang, M.; Huang, B.; Liu, R.; Zhao, J. Graphene supported Pt–Co alloy nanoparticles as cathode catalyst for microbial fuel cells. *Int. J. Electrochem. Sci.* **2013**, *8*, 149–158.
5. Cetinkaya, A.Y.; Ozdemir, O.K.; Koroglu, E.O.; Hasimoglu, A.; Ozkaya, B. The development of catalytic performance by coating Pt–Ni on CMI7000 membrane as a cathode of a microbial fuel cell. *Bioresour. Technol.* **2015**, *195*, 188–193. [CrossRef] [PubMed]
6. Cui, C.H.; Li, H.H.; Liu, X.J.; Gao, M.R.; Yu, S.H. Surface composition and lattice ordering-controlled activity and durability of cupt electrocatalysts for oxygen reduction reaction. *ACS Catal.* **2012**, *2*, 916–924. [CrossRef]
7. Maiyalagan, T.; Khan, F.N. Electrochemical oxidation of methanol on Pt/V_2O_5–C composite catalysts. *Catal. Commun.* **2009**, *10*, 433–436. [CrossRef]
8. Liu, X.; Fu, G.; Chen, Y.; Tang, Y.; She, P.; Lu, T. Pt–Pd–Co trimetallic alloy network nanostructures with superior electrocatalytic activity towards the oxygen reduction reaction. *Chem. Eur. J.* **2014**, *20*, 585–590. [CrossRef] [PubMed]
9. Chu, D.; Gilman, S. Methanol electro-oxidation on unsupported Pt–Ru alloys at different temperatures. *J. Electrochem. Soc.* **1996**, *143*, 1685–1690. [CrossRef]
10. Sun, H.J.; Ding, L.X.; Chen, Y.; Zhou, Y.M.; Lu, T.H.; Tang, Y.W. Changes of composition and structure of Pt–Ru/C catalyst in the methanol electro-oxidation process. *Chin. J. Inorg. Chem.* **2010**, *26*, 25–28.
11. Chen, Y.; Zhou, Y.; Tang, Y.; Lu, T. Electrocatalytic properties of carbon-supported Pt–Ru catalysts with the high alloying degree for formic acid electrooxidation. *J. Power Sources* **2010**, *195*, 4129–4134. [CrossRef]

12. Paulus, U.; Schmidt, T.; Gasteiger, H.; Behm, R. Oxygen reduction on a high-surface area Pt/vulcan carbon catalyst: A thin-film rotating ring-disk electrode study. *J. Electroanal. Chem.* **2001**, *495*, 134–145. [CrossRef]
13. Mayrhofer, K.; Blizanac, B.; Arenz, M.; Stamenkovic, V.; Ross, P.; Markovic, N. The impact of geometric and surface electronic properties of Pt-catalysts on the particle size effect in electrocatalysis. *J. Phys. Chem. B* **2005**, *109*, 14433–14440. [CrossRef] [PubMed]
14. Zhou, W.P.; Lewera, A.; Larsen, R.; Masel, R.I.; Bagus, P.S.; Wieckowski, A. Size effects in electronic and catalytic properties of unsupported palladium nanoparticles in electrooxidation of formic acid. *J. Phys. Chem. B* **2006**, *110*, 13393–13398. [CrossRef] [PubMed]
15. Liu, Z.; Lee, J.Y.; Han, M.; Chen, W.; Gan, L.M. Synthesis and characterization of Pt–Ru/C catalysts from microemulsions and emulsions. *J. Mater. Chem.* **2002**, *12*, 2453–2458. [CrossRef]
16. Wagner, C.; Naumkin, A.; Kraut-Vass, A.; Allison, J.; Powell, C.; Rumble, J., Jr. National Institute of Standard & Technology, X-ray Photoelectron Spectroscopy Database, Nist Standard Reference Database 20, Version 3.2 (Web Version). Available online: http://srdata.nist.gov/xps/ (accessed on 6 June 2000).
17. Ye, F.; Liu, H.; Hu, W.; Zhong, J.; Chen, Y.; Cao, H.; Yang, J. Heterogeneous Au-Pt nanostructures with enhanced catalytic activity toward oxygen reduction. *Dalton Trans.* **2012**, *41*, 2898–2903. [CrossRef] [PubMed]
18. Qu, J.; Liu, H.; Ye, F.; Hu, W.; Yang, J. Cage-bell structured Au-Pt nanomaterials with enhanced electrocatalytic activity toward oxygen reduction. *Int. J. Hydrog. Energy* **2012**, *37*, 13191–13199. [CrossRef]
19. Hu, Y.M.; Zhu, A.M.; Zhang, C.L.; Zhang, Q.G.; Liu, Q.L. Microwave-assisted synthesis of double-shell PtRu/TiO_2 catalyst towards methanol electro-oxidation. *Int. J. Hydrog. Energy* **2015**, *40*, 15652–15662. [CrossRef]
20. Yang, J.; Chen, X.; Ye, F.; Wang, C.; Zheng, Y.; Yang, J. Core-shell CdSe@ Pt nanocomposites with superior electrocatalytic activity enhanced by lateral strain effect. *J. Mater. Chem.* **2011**, *21*, 9088–9094. [CrossRef]
21. Marković, N.M.; Gasteiger, H.A.; Ross, P.N.; Jiang, X.; Villegas, I.; Weaver, M.J. Electro-oxidation mechanisms of methanol and formic acid on Pt–Ru alloy surfaces. *Electrochim. Acta* **1995**, *40*, 91–98. [CrossRef]
22. Stojmenovic, M.; Momcilovic, M.; Gavrilov, N.; Pasti, I.A.; Mentus, S.; Jokic, B.; Babic, B. Incorporation of Pt, Ru and Pt–Ru nanoparticles into ordered mesoporous carbons for efficient oxygen reduction reaction in alkaline media. *Electrochim. Acta* **2015**, *153*, 130–139. [CrossRef]
23. Zhang, J.; Vukmirovic, M.B.; Sasaki, K.; Nilekar, A.U.; Mavrikakis, M.; Adzic, R.R. Mixed-metal Pt monolayer electrocatalysts for enhanced oxygen reduction kinetics. *J. Am. Chem. Soc.* **2005**, *127*, 12480–12481. [CrossRef] [PubMed]
24. Ghasemi, M.; Ismail, M.; Kamarudin, S.K.; Saeedfar, K.; Daud, W.R.W.; Hassan, S.H.; Heng, L.Y.; Alam, J.; Oh, S.-E. Carbon nanotube as an alternative cathode support and catalyst for microbial fuel cells. *Appl. Energy* **2013**, *102*, 1050–1056. [CrossRef]
25. Wen, Q.; Wang, S.; Yan, J.; Cong, L.; Chen, Y.; Xi, H. Porous nitrogen-doped carbon nanosheet on graphene as metal-free catalyst for oxygen reduction reaction in air-cathode microbial fuel cells. *Bioelectrochemistry* **2014**, *95*, 23–28. [CrossRef] [PubMed]
26. Liu, Q.; Zhou, Y.; Chen, S.; Wang, Z.; Hou, H.; Zhao, F. Cellulose-derived nitrogen and phosphorus dual-doped carbon as high performance oxygen reduction catalyst in microbial fuel cell. *J. Power Sources* **2015**, *273*, 1189–1193. [CrossRef]
27. He, W.; Zhang, X.; Liu, J.; Zhu, X.; Feng, Y.; Logan, B.E. Microbial fuel cells with an integrated spacer and separate anode and cathode modules. *Environ. Sci. Water Res. Technol.* **2016**, *2*, 186–195. [CrossRef]
28. Dong, H.; Yu, H.; Wang, X.; Zhou, Q.; Feng, J. A novel structure of scalable air-cathode without nafion and Pt by rolling activated carbon and PTFE as catalyst layer in microbial fuel cells. *Water Res.* **2012**, *46*, 5777–5787. [CrossRef] [PubMed]
29. Yang, G.; Chen, Y.; Zhou, Y.; Tang, Y.; Lu, T. Preparation of carbon supported Pd–P catalyst with high content of element phosphorus and its electrocatalytic performance for formic acid oxidation. *Electrochem. Commun.* **2010**, *12*, 492–495. [CrossRef]
30. Li, Y.; Zhou, W.; Wang, H.; Xie, L.; Liang, Y.; Wei, F.; Idrobo, J.-C.; Pennycook, S.J.; Dai, H. An oxygen reduction electrocatalyst based on carbon nanotube-graphene complexes. *Nat. Nanotech.* **2012**, *7*, 394–400. [CrossRef] [PubMed]
31. Watson, V.J.; Nieto Delgado, C.; Logan, B.E. Influence of chemical and physical properties of activated carbon powders on oxygen reduction and microbial fuel cell performance. *Environ. Sci. Technol.* **2013**, *47*, 6704–6710. [CrossRef] [PubMed]

32. Yang, G.; Sun, Y.; Yuan, Z.; Lü, P.; Kong, X.; Li, L.; Chen, G.; Lu, T. Application of surface-modified carbon powder in microbial fuel cells. *Chin. J. Catal.* **2014**, *35*, 770–775. [CrossRef]
33. Thygesen, A.; Poulsen, F.W.; Angelidaki, I.; Min, B.; Bjerre, A.B. Electricity generation by microbial fuel cells fuelled with wheat straw hydrolysate. *Biomass Bioenergy* **2011**, *35*, 4732–4739. [CrossRef]
34. Clesceri, L.S.; Eaton, A.D.; Greenberg, A.E.; American Public Health Association. *Standard Methods for the Examination of Water Wastewater*; American Public Health Association: Washington, DC, USA, 1998.